A high order conservative method for the simulation of compressible multiphase flows

Vincent Perrier, Erwin Franquet

European Congress on Computational Methods
in Applied Sciences and Engineering (ECCOMAS 2012)
J. Eberhardsteiner et.al. (eds.)
Vienna, Austria, September 10-14, 2012

A HIGH-ORDER CONSERVATIVE METHOD FOR THE SIMULATION OF COMPRESSIBLE MULTIPHASE FLOWS

V. Perrier[1], **E. Franquet**[2]

[1]Inria Bordeaux Sud-Ouest, CAGIRE team and Laboratoire de Mathématiques et de leurs applications, UMR CNRS 5142, Université de Pau et des Pays de l'Adour, Avenue de l'Université, 64 013 Pau Cedex
e-mail: vincent.perrier@inria.fr

[2] LaTEP-ENSGTI, Université de Pau et des Pays de l'Adour, Bâtiment d'Alembert, rue Jules Ferry, 64 075 Pau Cedex, and Inria Bordeaux Sud-Ouest, CAGIRE team
e-mail: erwin.franquet@univ-pau.fr

Keywords: compressible flows, multiphase flows, high order method, interface flows

Abstract. *In this paper, we summarize the work published in [1, 2, 3]. Based on a simple stochastic model, a general framework for modelling diffuse interface flows is derived. This allows to both define a continuous Baer and Nunziato type model depending only on one free parameter, and to derive a numerical scheme, which is actually a discontinuous Galerkin extension of [4]. The numerical scheme is tested with interface flows, regular and nonregular multiphase flows.*

1 INTRODUCTION

One phase inviscid compressible flows are described by Euler's system, which accounts for the conservation of mass, momentum, and energy

$$\left\{\begin{array}{c} \partial_t \rho + \mathrm{div}_{\mathbf{x}}\left(\rho \mathbf{u}\right) = 0 \\ \partial_t \left(\rho \mathbf{u}\right) + \mathrm{div}_{\mathbf{x}}\left(\rho \mathbf{u} \otimes \mathbf{u} + P\right) = 0 \\ \partial_t \left(\rho E\right) + \mathrm{div}_{\mathbf{x}}\left(\left(\rho E + P\right)\mathbf{u}\right) = 0 \end{array}\right. \tag{1}$$

where ρ is the density, $\mathbf{u}$ the velocity, P the pressure, E the total specific energy, $E = \varepsilon + \frac{|\mathbf{u}|^2}{2}$, and ε is the specific internal energy, which is linked with the pressure and density by an equation of state $\varepsilon = \varepsilon(P, \rho)$. System (1) will be shortly denoted as

$$\partial_t \mathbf{U} + \mathrm{div}_{\mathbf{x}} \mathbf{F}(\mathbf{U}) = 0$$

As far as averaged multiphase flows are concerned, the following system can be considered [5]

$$\begin{array}{l} \dfrac{\partial\, \alpha_k}{\partial t} + \mathbf{u}_I \cdot \nabla \alpha_k = \mu(P_k - P_{\bar{k}}) \\ \dfrac{\partial \left(\alpha_k \rho_k\right)}{\partial\, t} + \mathrm{div}_{\mathbf{x}}\big(\alpha_k \rho_k \mathbf{u}_k\big) = 0 \\ \dfrac{\partial \left(\alpha_k \rho_k \mathbf{u}_k\right)}{\partial\, t} + \mathrm{div}_{\mathbf{x}}\big(\alpha_k \rho_k \mathbf{u}_k \otimes \mathbf{u}_k\big) + \nabla(\alpha_k P_k) = P_I \nabla \alpha_k + \lambda(\mathbf{u}_{\bar{k}} - \mathbf{u}_k) \\ \dfrac{\partial \left(\alpha_k \rho_k E_k\right)}{\partial\, t} + \mathrm{div}_{\mathbf{x}}\big(\alpha_k(\rho_k E_k + P_k)\mathbf{u}_k\big) = P_I \mathbf{u}_I \cdot \nabla \alpha_k - \mu P_I (P_k - P_{\bar{k}}) \\ \qquad\qquad\qquad\qquad\qquad\qquad\qquad\qquad\qquad\qquad + \lambda \mathbf{u}_I (\mathbf{u}_{\bar{k}} - \mathbf{u}_k) \end{array} \tag{2}$$

where α_k denotes the volume fraction, $\mathbf{u}_I$ is the local interfacial velocity, P_I is the local interfacial pressure, and λ and μ are relaxation parameters. System (2) raises the following problems:

1. Interfacial values (velocity and pressure) as well as relaxation parameters must be defined.

2. The system is not conservative and therefore it is not easy to derive a finite volume method. Logically, the derivation of a discontinuous Galerkin method is even more complicated, because this method basically consists in using finite volume fluxes on the boundaries, and continuous integrals inside the cells.

Many numerical methods have been derived for (2), see for example [6, 7], or [8] for a discontinuous Galerkin version, but in all of them, the Baer and Nunziato approximation is considered, i.e. $P_I = P_1$ and $\mathbf{u}_I = \mathbf{u}_2$. This approximation simplifies the system, because all the difficulties are concentrated on the solid contact wave, but it holds only in very special cases where one of the phase is nearly incompressible.

This paper is organized as follows. In the first part, we derive a Baer and Nunziato model, and give an explicit formulation of the interfacial pressure and velocity and a nonlinear formulation of the relaxation terms. In the isotropic and acoustic approximations, the only free parameter of the resulting system is a common factor of the relaxation terms. In the second part, a numerical scheme is derived with the same type of modelling. This actually revisits the scheme derived in [4], and with the continous limit previously computed, we can apply the framework of [9] for deriving a discontinous Galerkin scheme for our system. The numerical scheme is tested on cases involving interface flows, multiphase flows, and reactive flows.

2 MODEL DERIVATION USING A STOCHASTIC APPROACH

The aim of this section is to derive (nearly) explicitly the model (2). In [10], the derivation of (2) is explained by using ensemble average: knowing the local volume fraction of the fluids, a possible topology is rebuilt. If the topology is known, the equations are explicit, but depend on this topology. The last step consists in averaging the equations on "all" the possible topologies. For one realization of the topology, χ_k denotes the characteristic function ($\chi_k = 1$ inside the fluid k, and 0 elsewhere). Then

$$\chi_k \left(\partial_t \mathbf{U}_k + \mathrm{div}_{\mathbf{x}} \mathbf{F}_k(\mathbf{U}_k)\right) \;=\; 0 \tag{3}$$

and if $\mathbf{u}_i$ denotes the local interfacial velocity, then

$$\partial_t \chi_k + \mathbf{u}_i \cdot \nabla \chi_k \;=\; 0 \tag{4}$$

By combining (3) and (4), we may obtain:

$$\frac{\partial\, \chi_k \mathbf{U}_k}{\partial\, t} + \mathrm{div}_{\mathbf{x}}\Big(\chi_k \mathbf{F}_k(\mathbf{U}_k)\Big) - \Big(\mathbf{F}_k(\mathbf{U}_k) - \mathbf{u}_i \mathbf{U}_k\Big)\nabla \chi_k \;=\; 0 \tag{5}$$

2.1 Modelling the topology

For a given average $(\mathbf{x}, t) \mapsto \alpha_1(\mathbf{x}, t)$ of χ_1, we suppose that

$$\chi_1 = \frac{1 + \mathrm{sgn}(g_{\mathbf{x}})}{2}$$

where $g_{\mathbf{x}}$ is a Gaussian random process. For the sake of simplicity, we suppose that $\mathrm{Var}(g_x) = 1$ for all $\mathbf{x}$. We denote by $m(\mathbf{x})$ its mean. The constraint $\mathbb{E}\{\chi_1\} = \alpha_1$ (where $\mathbb{E}$ denotes the mathematical expectancy) induces:

$$\mathbb{E}\{\chi_1\} = \frac{1}{\sqrt{2\pi}} \int_{\mathbb{R}} \frac{1 + \mathrm{sgn}(g)}{2}\, \mathrm{e}^{-(g - m(\mathbf{x},t))^2/2}\, \mathrm{d}g = \frac{1}{\sqrt{2\pi}} \int_{\mathbb{R}} \frac{1 + \mathrm{sgn}(u + m(\mathbf{x},t))}{2}\, \mathrm{e}^{-g^2/2}\, \mathrm{d}g$$

which leads to

$$\alpha_1(\mathbf{x}, t) = \frac{1}{\sqrt{2\pi}} \int_{-m(\mathbf{x},t)}^{\infty} \mathrm{e}^{-g^2/2}\, \mathrm{d}g \tag{6}$$

This last equation uniquely defines $(\mathbf{x}, t) \mapsto m(\mathbf{x}, t)$, which has the same regularity as α_k. Last, for ensuring that χ_1 can be derived, we suppose that the autocorrelation function R of $g_{\mathbf{x}}$ can be derived at least twice, and that $R'(0) = 0$. The variables $\mathbf{U}_k(\mathbf{x}, t)$ are supposed to be deterministic. As a consequence, the derivation operators with respect to t and $\mathbf{x}$ for the two first terms of (5) are commutating. The only term that raises a problem is the third one of (5).

2.2 Computation of the third term of (5)

This term is tricky, because χ_1 is the image of a Gaussian random process by a non regular function, and because it depends on $\mathbf{u}_i$, which shall be defined. Definition of $\mathbf{u}_i$ actually depends on the direction of $\nabla \chi_1$: as shown on Figure 1, if the boundary of the set $\chi_1 = 0$ is regular, then the interface velocity is defined by solving the Riemann problem between phase 0 and phase 1 in the direction of $\nabla \chi_1$. The value of $\Big(\mathbf{F}_k(\mathbf{U}_k) - \mathbf{u}_i \mathbf{U}_k\Big)$ is also taken at the interface. For a given direction $\mathbf{n}$, we denote by $\mathbf{U}^\star$ the state on one part of the contact surface, and by $u^\star_{\mathbf{n}}$ the normal velocity on one part of the contact surface. Then

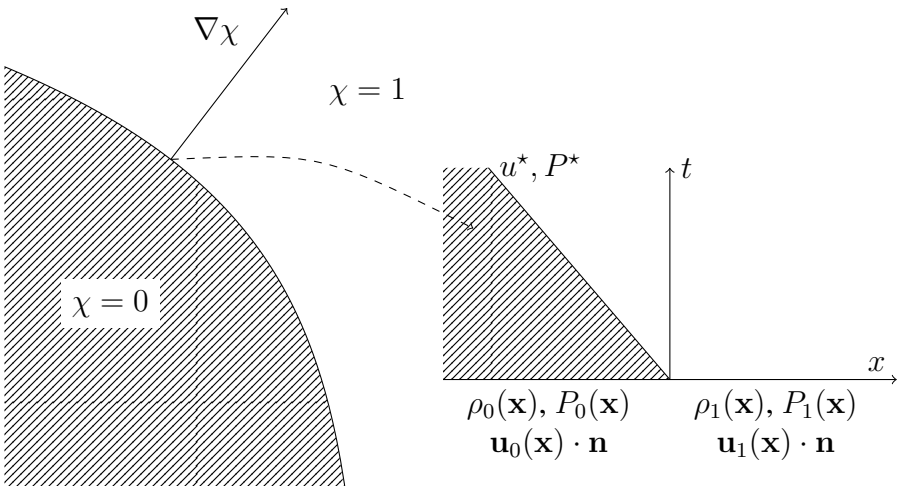

Figure 1: Local interface variables. If the boundary between the two phases is $\mathscr{C}^1$, then we may define the interfacial velocity and pressure by solving a local Riemann problem. We define by $\mathbf{n}$ the unit vector that has the same direction and sense as $\nabla\chi$. Then we can define the interfacial pressure and velocity as $P_I = P^\star$ and $\mathbf{u}_I = u^\star\mathbf{n}$.

$$\Big(\mathbf{F}_k(\mathbf{U}_k) - \mathbf{u}_i\mathbf{U}_k\Big)\cdot\mathbf{n} = \begin{pmatrix} \rho^\star u^\star_{\mathbf{n}} \\ \rho^\star u^\star_{\mathbf{n}}\mathbf{u}^\star + P^\star\mathbf{n} \\ (\rho^\star E^\star + P^\star)u^\star_{\mathbf{n}} \end{pmatrix} - u^\star_{\mathbf{n}}\begin{pmatrix} \rho^\star \\ \rho^\star\mathbf{u}^\star \\ \rho^\star E^\star \end{pmatrix} = \begin{pmatrix} 0 \\ P^\star\mathbf{n} \\ P^\star u^\star_{\mathbf{n}} \end{pmatrix} = \mathbf{F}^{\mathrm{lag}}(\mathbf{n}) \quad (7)$$

Note that in (7), the value does not depend on which side of the contact $\mathbf{U}^\star$ is taken.

Under sufficient condition on the process $g_{\mathbf{x}}$, $\nabla\chi_k$ exists, and computing it is equivalent to computing up and downcrossings of $g_{\mathbf{x}}$. Computing these up and downcrossings is usual for a centered Gaussian process, see [11, 12]. With this, we can find in one dimension

$$\mathbb{E}\left\{(\mathbf{F}(\mathbf{U}_k) - \mathbf{u}_i\mathbf{U}_k)\cdot\nabla\chi_k\right\} = \mathbf{F}^{\mathrm{lag}}(\nabla\alpha_k) + \frac{\sqrt{-R''(0)}}{2\pi}\left(\mathbf{F}^{\mathrm{lag}}(\bar{k},k) - \mathbf{F}^{\mathrm{lag}}(k,\bar{k})\right) \quad (8)$$

where $\mathbf{F}^{\mathrm{lag}}(i,j)$ is the Lagrangian flux found in (7) with the fluid i on the left and the fluid j on the right. The first part comes from the average of χ_k, whereas the second part comes from the computation of the up and down crossings of $g_{\mathbf{x}} - m(\mathbf{x})$. Equation (8) gives an explicit closure for the interface varables

$$\begin{cases} \mathbf{u}_I = u^\star(\nabla\alpha_1)\mathbf{n}(\nabla\alpha_1) \\ P_I = P^\star(\nabla\alpha_1) \end{cases} \quad (9)$$

and a nonlinear version of the relaxation terms.

The resulting system depends on only one modelling parameter, $R''(0)$, which is a common factor of the relaxation parameters λ and μ of (2).

In two dimensions, the same computation can be made. The computation of upcrossing and downcrossing of a Gaussian process is known provided the joint law of $g_{\mathbf{x}}$ and its derivative can be computed. In two dimensions, it is necessary to know the joint law of $g_{\mathbf{x}}$ and its derivative *in both directions*. The general expression of the covariance matrix of this joint law is

$$\mathscr{C} = \begin{pmatrix} 1 & 0 & 0 \\ 0 & -\partial_{xx}R(0) & -\partial_{xy}R(0) \\ 0 & -\partial_{xy}R(0) & -\partial_{yy}R(0) \end{pmatrix}$$

and the joint law is $\dfrac{1}{(2\pi)^{3/2}\sqrt{\det \mathscr{C}}} \exp\left(-\dfrac{1}{2}\,\eta^T \mathscr{C}^{-1}\eta\right)\,\mathrm{d}\eta$. This law can be put into the following form by changing the coordinates (η_2, η_3) into polar coordinates

$$\frac{1}{(2\pi)^{3/2}\sqrt{\det \mathscr{C}}} \exp\left(-\frac{\eta_1^2}{2}\right) \exp\left(-\frac{r^2\,\varphi(\theta)}{2\det \mathscr{C}}\right)\,\mathrm{d}\eta_1\, r\mathrm{d}r\mathrm{d}\theta$$

with $\varphi(\theta) = -\partial_{yy}R(0)\cos^2\theta - \partial_{yy}R(0)\sin^2\theta + 2\partial_{xy}R(0)\sin\theta\cos\theta$. This allows to compute the probability of an upcrossing in the direction θ. Then the third term of (5) in two dimensions is

$$\mathbb{E}\left\{(\mathbf{F}(\mathbf{U}_k) - \mathbf{u}_i\mathbf{U}_k)\cdot\nabla\chi_k\right\} = \mathbf{F}^{\mathrm{lag}}(\nabla\alpha_k) + \frac{\det \mathscr{C}}{4\pi}\int_0^\pi \frac{\left(\mathbf{F}^{\mathrm{lag}}(\mathbf{n}(\theta)) + \mathbf{F}^{\mathrm{lag}}(-\mathbf{n}(\theta))\right)}{\varphi(\theta)^{3/2}}\,d\theta \quad (10)$$

This gives a full nonlinear expression for the two dimensional relaxation terms of (2). Actually, the relaxation terms of (2) can be recovered provided the covariance matrix is diagonal and the acoustic approximation holds. In this case, the diagonal hypothesis on $\mathscr{C}$ induces

$$\mathscr{C} = \begin{pmatrix} \xi & 0 \\ 0 & \xi \end{pmatrix} \qquad \text{and} \qquad \varphi(\theta) = \xi$$

so that

$$\frac{\det \mathscr{C}}{4\pi}\int_0^\pi \frac{\left(\mathbf{F}^{\mathrm{lag}}(\mathbf{n}(\theta)) + \mathbf{F}^{\mathrm{lag}}(-\mathbf{n}(\theta))\right)}{\varphi(\theta)^{3/2}}\,d\theta = \frac{\sqrt{\xi}}{4\pi}\int_0^\pi \left(\mathbf{F}^{\mathrm{lag}}(\mathbf{n}(\theta)) + \mathbf{F}^{\mathrm{lag}}(-\mathbf{n}(\theta))\right)\,d\theta$$

In the acoustic approximation, $P^\star$ and $u^\star$ in the direction $\mathbf{n}$ of (7) can be expressed as

$$\begin{cases} P^\star = \dfrac{Z_2P_1 + Z_1P_2}{Z_1+Z_2} + \dfrac{Z_1Z_2\,(\mathbf{u}_2-\mathbf{u}_1)\cdot\mathbf{n}}{Z_1+Z_2} \\ u^\star = \dfrac{Z_1\mathbf{u}_1\cdot\mathbf{n} + Z_2\mathbf{u}_2\cdot\mathbf{n} + P_2 - P_1}{Z_1+Z_2} \end{cases} \quad (11)$$

where Z_i is the acoustic impedance, $Z_i = \rho_i c_i$, and consequently the relaxation terms are

$$\frac{\sqrt{\xi}}{4(Z_1+Z_2)}\begin{pmatrix} P_2 - P_1 \\ 0 \\ \dfrac{Z_1Z_2}{2}\,(\mathbf{u}_2-\mathbf{u}_1) \\ \dfrac{2(Z_2P_1+Z_1P_2)}{Z_1+Z_2}\,(P_2-P_1) + \dfrac{Z_1Z_2\,(Z_1\mathbf{u}_1+Z_2\mathbf{u}_2)\cdot(\mathbf{u}_2-\mathbf{u}_1)}{Z_1+Z_2} \end{pmatrix}$$

These relaxation terms depend on only one modelling parameter: ξ. Besides, in the energy equation, we do not recover relaxation terms as in (2), because

$$\frac{2(Z_2P_1+Z_1P_2)}{Z_1+Z_2} \qquad \text{and} \qquad \frac{Z_1Z_2\,(Z_1\mathbf{u}_1+Z_2\mathbf{u}_2)}{Z_1+Z_2}$$

do not exactly match with the expression of P_I and $\mathbf{u}_I$ in the acoustic approximation.

2.3 About the relaxation parameter

We dwell on the physical meaning of this parameter. On one hand, the autocovariance function measures the memory of the process: if R quickly goes to 0, the process has a short memory, which means that the media are well mixed; on the other hand, the higher $|R''(0)|$ is, the quicker velocities and pressure are relaxed. Looking at the second order approximation of R gives

$$R(\tau) = 1 + \frac{R''(0)}{2}\,\tau^2 + o\left(\tau^2\right)$$

where $R''(0)$ is negative. In this approximation, the higher $|R''(0)|$ is, the quicker R goes to 0. This means that velocities and pressure relax quicker with a short range memory process, which matches with well mixed fluids. This is physically relevant.

For fully closing the system, we would like to know the value of $R''(0)$, which is the covariance of $g_{\mathbf{x}}$. We would like to point out that equations (3) and (4) cannot give any information on the evolution of $R''(0)$, because all the moments of χ_k are equal to the average of χ_k; as a consequence, evolution of R'' must be given by a model.

3 DERIVATION OF THE NUMERICAL SCHEME

Using the idea of [4], we propose to first discretize (3) and (4) instead of (2).

It is well known that system (2), although being hyperbolic, cannot be written in conservative form. The direct definition of the jump relations across shock waves is thus not available. To circumvent this issue in the case of a Baer and Nunziato closure ($\mathbf{u}_I = \mathbf{u}_2$ and $P_I = P_1$), some authors proposed either an algebraic relation [6] or a combination of an explicit solution with the formulation of [9] for DG methods with nonconservative terms [8]. Another approach was developed in [2] which is briefly recalled hereafter.

It thus has been shown that the DG formulation of (5), using the framework of [9] and after averaging among the realizable topologies, expresses:

$$\begin{aligned}
\frac{\partial\,\mathbb{E}\left\{\chi_k \mathbf{U}_k\right\}}{\partial\, t} \quad &+ \quad \sum_{K\in\mathcal{T}_h}\int_K -\,\mathbb{E}\left\{\chi_k \mathbf{F}(\mathbf{U})\right\}\nabla\varphi + \varphi\left(\mathbb{E}\left\{(\mathbf{F}-\mathbf{u}_i\mathbf{U})\nabla\chi_k\right\}\right) && (12)\\
&- \quad \sum_{S\in S_i}\int_S [\![\,\varphi\,]\!]\,\{\!\{\,\mathbb{E}\left\{\chi_k \mathbf{F}_k(\mathbf{U}_k)\right\}\,\}\!\}\cdot\mathbf{n}^S && (13)\\
&+ \quad \sum_{S\in S_i}\int_S \{\!\{\,\varphi\,\}\!\}\int_0^1 \frac{\partial\Phi}{\partial s}(s,u^L,u^R)\mathbb{E}\left\{\left(\mathbf{F}_k(\mathbf{U}_k)-\mathbf{u}_i\mathbf{U}_k\right)\nabla\chi_k\right\}\cdot\mathbf{n}^S && (14)\\
&+ \quad \sum_{S\in S_b}\int_S \varphi\mathbb{E}\left\{\chi_k\mathbf{F}(\mathbf{U})\right\}\cdot\mathbf{n}^{\text{out}} = 0 && (15)
\end{aligned}$$

Here, Φ is a path connecting the left state L and the right state R (whose definition is given in [13]), $[\![\,\varphi\,]\!] = \varphi^R - \varphi^L$ and $\{\!\{\,\varphi\,\}\!\} = \dfrac{\varphi^R+\varphi^L}{2}$, and finally $\mathbb{E}$ is a mathematical expectancy.

The main issues lie in the expression of the boundary integrals (13) and (14) and in the cell integrals (12). To overcome these difficulties, we use in [1, 2] the method of [4] to compute the

fluxes at the boundaries :

$$\int_S [\![\varphi]\!] \{\!\{ \mathbb{E}\left\{\chi_k \mathbf{F}_k(\mathbf{U}_k)\right\} \}\!\} \cdot \mathbf{n}^S \approx \int_S [\![\varphi]\!] \mathcal{F}^{k,\text{eul},+} \tag{16}$$

$$\int_S \{\!\{ \varphi \}\!\} \int_0^1 \frac{\partial \Phi}{\partial s}(s, u^L, u^R) \mathbb{E}\left\{\left(\mathbf{F}_k(\mathbf{U}_k) - \mathbf{u}_i \mathbf{U}_k\right) \nabla \chi_k\right\} \cdot \mathbf{n}^S \approx \int_S \varphi^L \mathcal{F}^{k,\text{lag},-} + \int_S \varphi^R \mathcal{F}^{k,\text{lag},+} \tag{17}$$

Here, $\mathcal{F}^{k,\text{eul},+}$ and $\mathcal{F}^{k,\text{lag},\pm}$ are average of Eulerian and Lagrangian fluxes which are determined thanks to the average of the flux corresponding to the solutions of the Riemann problems occurring at the cell boundaries between each pure fluids.

If we now consider the term (12) corresponding to the cell integrals, we use a continuous formulation of the problem consistent with our above definition of the boundary integrals. It thus leads to:

$$\mathbb{E}\left\{(\mathbf{F}(\mathbf{U}) - \sigma \mathbf{U}) \cdot \nabla \chi_1\right\} = \begin{pmatrix} 0 \\ -P^\star(\nabla\alpha_1)\mathbf{n}(\nabla\alpha_1) \left\|\nabla\alpha_1\right\| \\ -u^\star(\nabla\alpha_1) P^\star(\nabla\alpha_1) \left\|\nabla\alpha_1\right\| \end{pmatrix} \tag{18}$$

Here, $P^\star$ and $u^\star$ are the pressure and velocity at the interface of the Riemann problem with direction $\mathbf{n}$ (left state corresponding to fluid 2 and right state to fluid 1), the unitary vector that has the same sense and direction as $\nabla\alpha_1$.

4 NUMERICAL RESULTS

4.1 Consistency test

A continuous system, which is consistent with (2) with closure (9) was found for the scheme [4]. This first test consists in a one dimensional regular solution. This solution is computed by imposing the volume fraction of one of the fluids, and then by supposing that the solution is self-similar and attached to the field $\mathbf{u}_I$. Then the exact solution is computed by the characteristic method: the variables of the initial solution at a point $\mathbf{x}$ are transported at the velocity $\mathbf{u}_I(\mathbf{x})$. The initial profile of the volume fraction is imposed as follows. If we denote by Ψ the function such that $\Psi'(x) = (x-1)^4(x+1)^4$ and $\Psi(0) = 0$. Ψ vanishes on -1 and 1 with a $\mathscr{C}^4$ regularity.

On the boundaries of the domain, α_2 takes the values $\alpha_2^{(L)}$ on the left and $\alpha_2^{(R)}$ on the right, and α_2 is then set to

$$\begin{cases} \alpha_2(x) = \alpha_2^{(L)} & \text{if} \quad x < x_1, \\ \alpha_2(x) = \alpha_2^{(L)} + \dfrac{\alpha_2^{(R)} - \alpha_2^{(L)}}{\Psi(1)} \Psi\left(\dfrac{x - \dfrac{x_1 + x_2}{2}}{\frac{x_2 - x_1}{2}}\right) & \text{if} \quad x_1 < x < x_2, \\ \alpha_2(x) = \alpha_2^{(R)} & \text{if} \quad x > x_2. \end{cases}$$

Other variables are numerically computed by solving an EDO system given by the fact that the initial solution is a self-similar solution attached to the field $\mathbf{u}_I$. Across this wave, $\mathbf{u}_I$ is checked to be increasing, so as to ensure that the characteristics are not crossing. The solution is computed on a family of meshes with 100, 200, 400 and 800 cells and is shown on Figure 2. The associated convergence orders are shown in Figure 3.

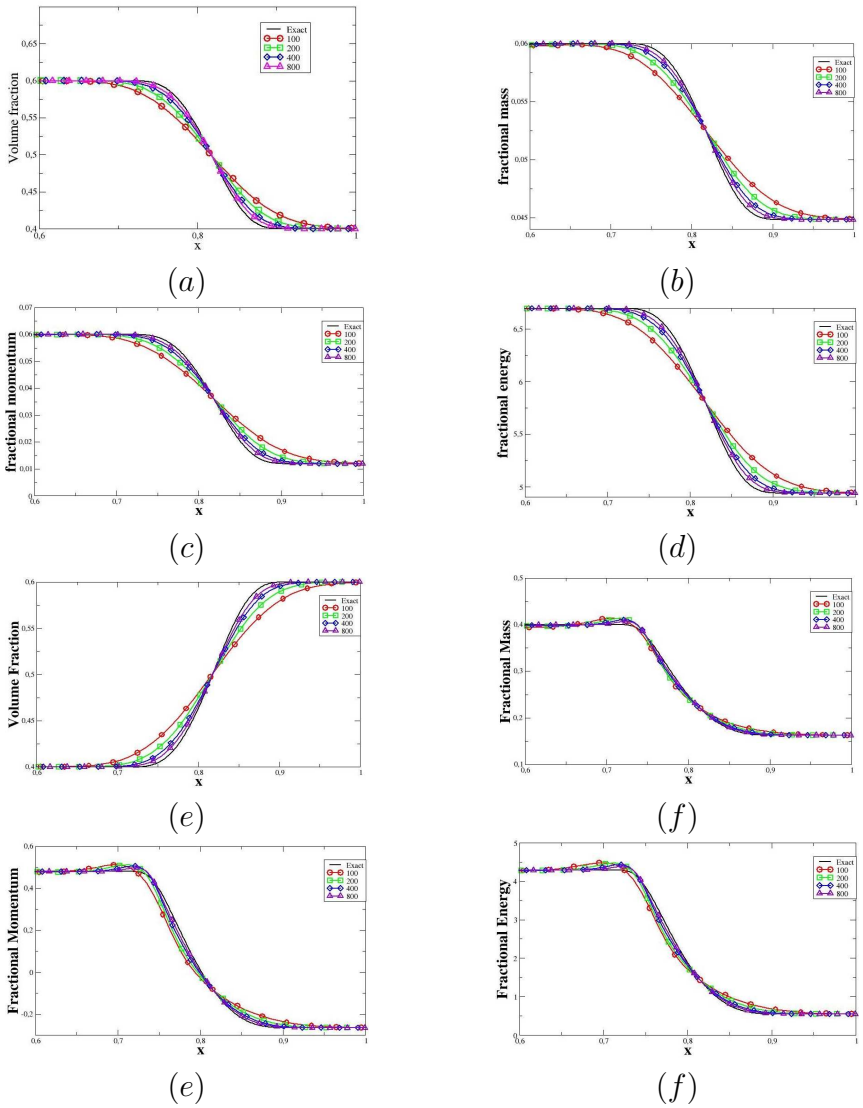

Figure 2: Results for the consistency test for all the variables. Exact solutions are compared with the solutions computed with 100, 200, 400 800 cells. Convergence to the exact solution is observed for all the variables of fluid 1 ((a),(b),(c),(d)), and of fluid 2 ((e),(f),(g),(h)).

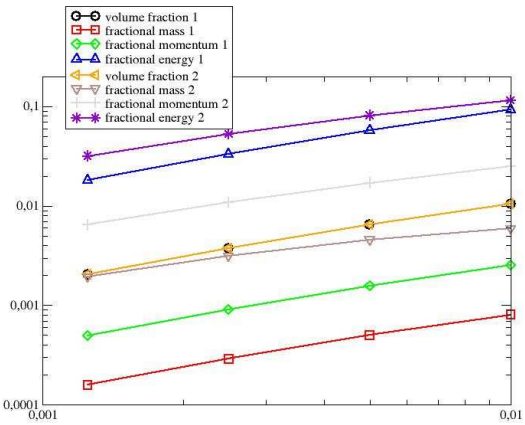

Figure 3: The convergence order of the consistency test is drawn for all the conservative variables computed: the L^2 error is computed for the mesh with 100, 200, 400 and 800 cells. For all the variables, the convergence is proved to be close to 1.

4.2 Multiphase vortex

In this case, we want to test accuracy of the solution when pressures and velocities are equal, but when the pressure is not uniform. The initial condition consists in a multiphase vortex (see [1, 8] for its expression). A constant horizontal velocity is added, and periodic boundary conditions are set on the left and on the right. In order to have a fair comparison between the different accuracies order, the higher degree we deal with, the coarser the mesh is; the number of degrees of freedom is kept nearly constant (about 1200 degrees of freedom). A slice along $x = 0$ comparing the different results is presented in Figure 4.

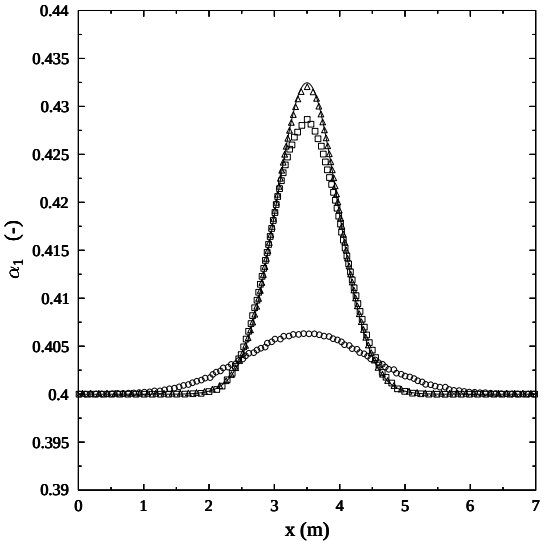

Figure 4: Slice of the multiphase vortex along the y-axis. Comparison of the volume fraction for the DG^0 (circle) and DG^1 (square) and DG^2 (triangle) solutions with the exact solution (line). In this test, the number of cells is 12314, 4092 and 2112, so that the number of degrees of freedom is nearly constant.

4.3 Multiphase shock tube

We are concerned here by a multiphase shock tube problem, where mixtures are initially present in both chambers. This example is inspired by [7], whose test 1 is re-used in the present study. It is worth highlighting that we do not solve the same continuous problem since the work of [7] deals with the Baer & Nunziato closure for system (2). In Fig. 5,the solution is presented at time $t = 0.1\,\mathrm{s}$ for a DG^1 solution computed on a 5000 cells mesh. We also show on the same figure the converged solution obtained with the DG^0 solution on a 10,000 cells mesh. We have a good agreement between each solution.

4.4 Shock-bubble interaction and Richtmyer-Meshkov instability

This last example deals with the well known problem of Quirk & Karni [14], based on the experiments of Haas & Sturtevant [15], of an incident plane shock wave impacting a spherical bubble, which is at a different density than the ambient fluid. The initial configuration is shown in Figure 6. The shocked state corresponds to a density of $1.92691\,\mathrm{kg}\cdot\mathrm{m}^{-3}$, a velocity of $-0.33361\,\mathrm{m}\cdot\mathrm{s}^{-1}$, and a pressure of $1.5698\,\mathrm{Pa}$, which implies that the shock wave's Mach number is 1.22. The air at rest has a density $\rho = 1.4\,\mathrm{kg}\cdot\mathrm{m}^{-3}$ and the helium a density $\rho = 0.25463\,\mathrm{kg}\cdot\mathrm{m}^{-3}$, corresponding to atmospheric conditions. Both fluids obey the perfect gas equation of state, with $\gamma = 1.4$ for air and $\gamma = 1.648$ for helium.

The interaction of the shock wave with the density discontinuity will lead to a Richtmyer-Meshkov instability, whose development is governed by the Atwood number. In the present case, of a negative Atwood number, we will have a reversal of the bubble that is then penetrated by a jet of surrounding fluid and then gives two vortex downstream of the flow. This test is runned on a 25761 unstructured triangular conforming mesh, with a CFL number of 0.3. In Figure 7, we show the mixture density contour and the associated isovalues at time $t = 230\,\mathrm{ms}$. We obtain qualitatively good results with both schemes, yet the reversal of the bubble and the interface are better described with the DG^1 solution.

General behavior of the bubble and in particular the growth of the instability is typical of a Richtmyer-Meshkov instability. In [1], a quantitative analysis was done on the experimental results of [16], which consists in a simple interaction of a shock with a perturbed interface. Comparison between numerical and experimental points are shown on Figure 8.

4.5 Interface flows

Interface flows can be considered with (2). In this case, the variables are not regular, because the volume fraction jumps from 0 to 1. As a consequence, our method, which is linear and high order, induces oscillations in the volume fraction. Nevertheless, advection of the volume fraction is made through the surface contact, which is a linearly degenerate wave, so that oscillations are not increased by this wave. That is why we can use the simple limiter introduced in [17, 18] for forcing the volume fraction to stay between 0 and 1.

Simple advection tests In these first tests, we consider simple advection problems

$$\partial_t u + \beta \cdot \nabla u = 0$$

Our first test is a one dimensional advection of a discontinuity. Convergence order is tested with and without slope limiting. Results are shown on Figure 9.

Our second test is Zalesaks' test [19], which is widely used for testing accuracy of level set methods. Results for this test are shown in Figure 10.

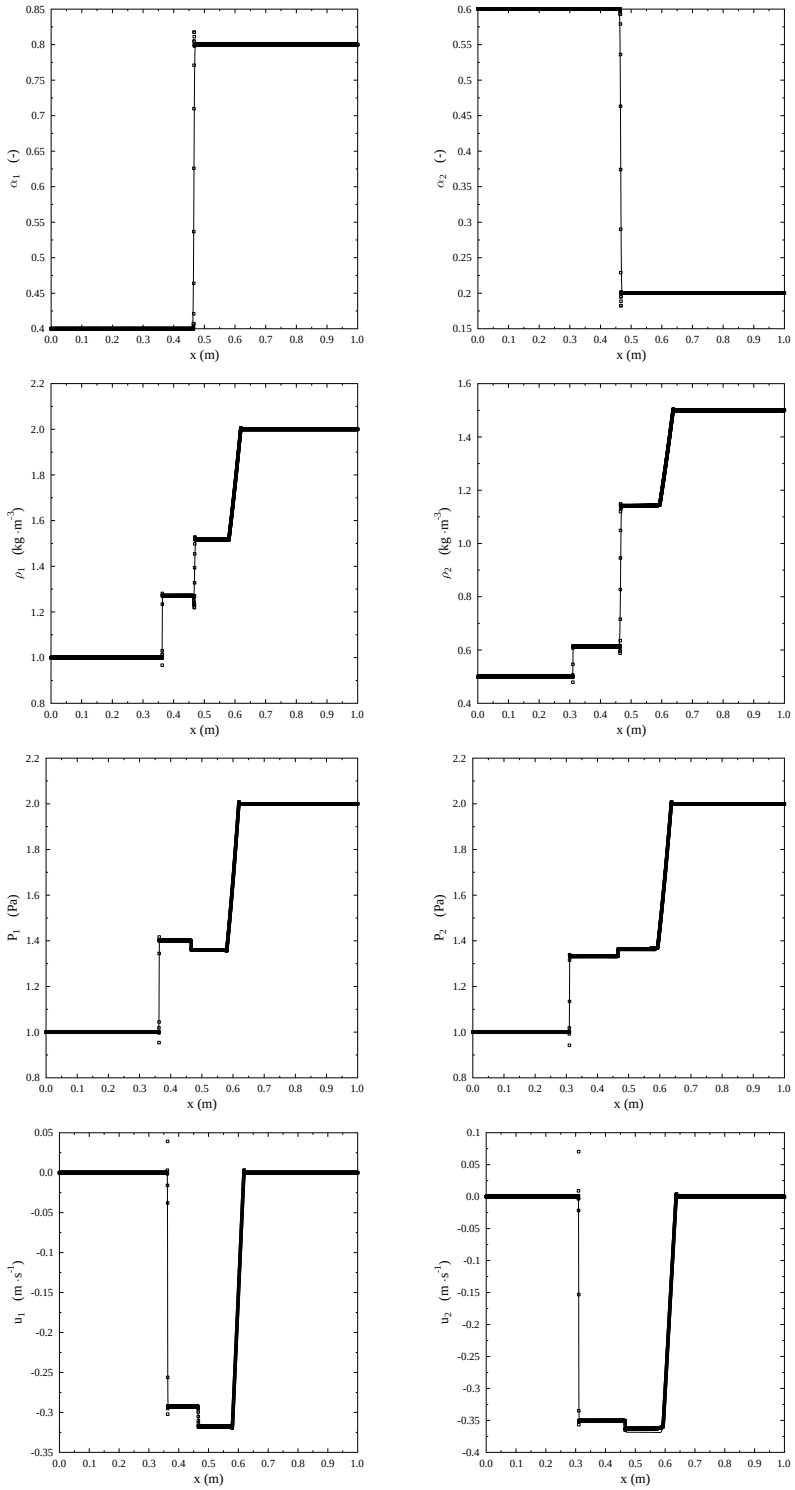

Figure 5: Multiphase shock tube: Comparison of the DG^1 (square) and the converged DG^0 (line) solution.

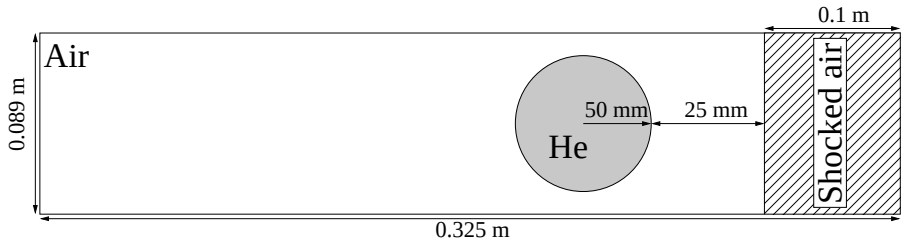

Figure 6: Computational domain for the shock bubble interaction.

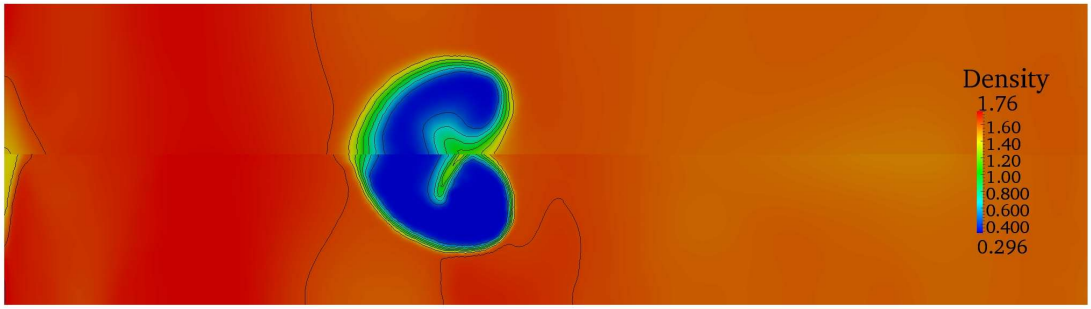

Figure 7: Interaction of a shock wave with an helium bubble in air. Contours of the mixture density for the DG^0 (top) and the DG^1 (bottom) schemes. Isovalues are also represented in black lines.

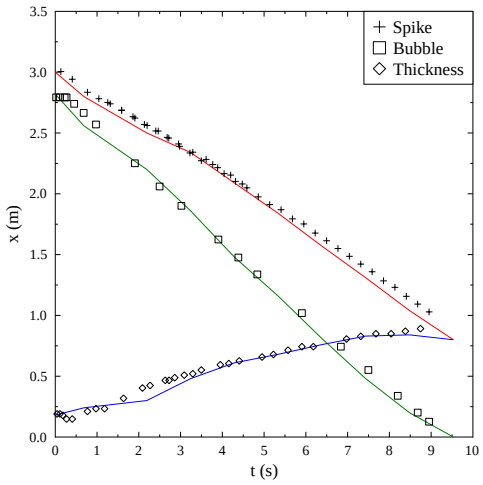

Figure 8: Richtmyer-Meshkov instability. Comparison of the time evolutions of characteristic positions for the DG^1 scheme (lines) and the results of [16] (symbols).

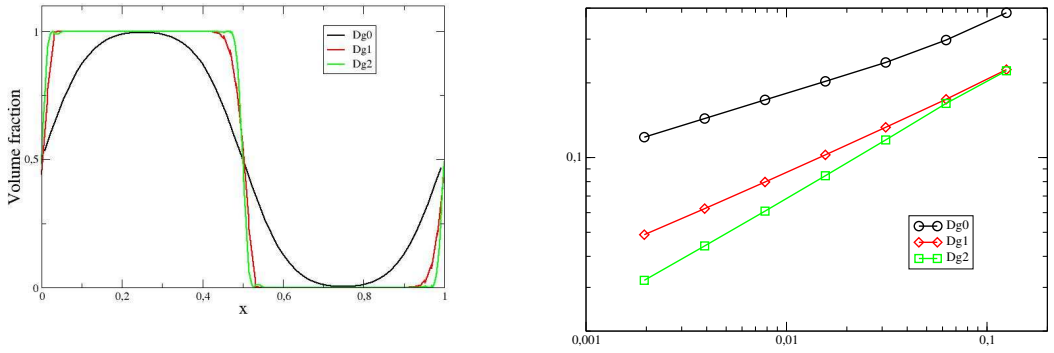

Figure 9: Solution obtained for the advection of a one dimensional discontinuity. On the left, results are shown for an approximation degree of 0, 1 and 2 on a mesh of 64 cells. On the right, the convergence error is represented on a log-log scale. We observe that the limiter used does not destroy the convergence order.

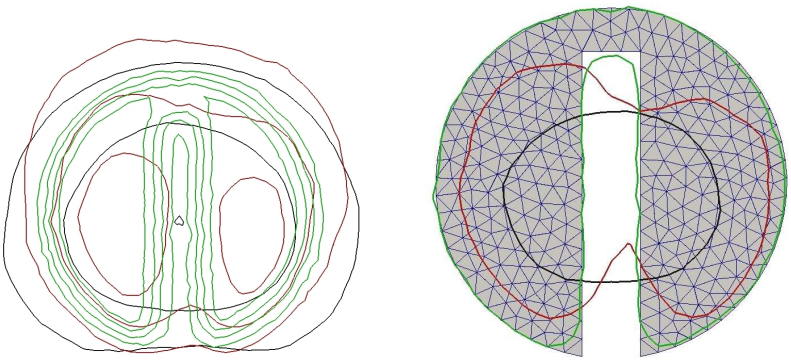

Figure 10: Results for Zalesak test. On the left figure, isovalues 0.2,0.4,0.6 and 0.8 are represented for the DG^0 (black), DG^1 (red) and DG^2 (green) computations. Some of these isovalues are not in the Figure because they are too far from the initial shape. On the right side, we draw the isovalue 0.5 of α_1, and we compare it with the initial shape. These two figures prove the much stronger accuracy of the DG^2 computations, which is the only one able to conserve the initial shape.

Rayleigh-Taylor instability In this test, a vertical gravity force is added to the momentum and energy equations. The Rayleigh-Taylor instability is observed when a heavy fluid lies on the top of a lighter fluid. Exact initial conditions for this test can be found in [2]. Adding the gravity to the system gives an hyperbolic system with source term. As explained in [20], the scheme must exactly conserve stationary solutions, otherwise, spurious oscillations appear. For ensuring conservation, an hydrostatic reconstruction is done, see [2] for details. Results for the Rayleigh-Taylor instability can be found in Figure 11. They show a very low diffusive behavior of the DG^2 solution.

4.6 Permeable fronts

In [3], the method was extended for taking into account permeable fronts following [21]. Our first test consists in a two-dimensional detonation front. A rectangular tank contains an explosive which is initially ignitiated in its center, so that a high pressure "bubble" of products is found here. Both fluids obey the stiffened gas equation of state, and the detonation velocity is computed using the Chapman-Jouguet closure. We present on Figure 12 the results obtained on a 855 triangles mesh, corresponding to a quarter of the rectangle.

Eventually, our last example is the propagation of a projectile in a liquid tank. In this test, the fluid is governed by the isothermal van-der-Waals equation of state. The main issue here is the dynamic apparition of a gaseous phase, which was not initially present. We present in Figure 13 the comparisons of the results between first and second order method.

5 CONCLUSION

In the first part, thanks to a simple stochastic model, an expression of the interfacial velocity and pressure, and a general nonlinear formulation of the relaxation terms for averaged multiphase flows were found. With more restrictive hypothesis on the flow (isotropy and acoustic approximation), linear relaxation terms found are very close of the ones of (2). In the second part, a Runge-Kutta discontinuous Galerkin method for this system was derived, based on the ideas of [9, 4]. This scheme was tested on multipase flows, interface flows, and reactive flows. As mentioned in [3], the slope limiting is not straightforward. To summarize:

- For interface flows, very good results can be obtained with the limiter of [17].
- If the velocities and pressure are equal, classical limiters can be used.
- In the case of reactive fronts, a limiter that is monotone for the volume fractions is mandatory, otherwise convergence to a wrong solution can be observed. This induces a strong constraint, because monotone limiters are known to flatten extrema.

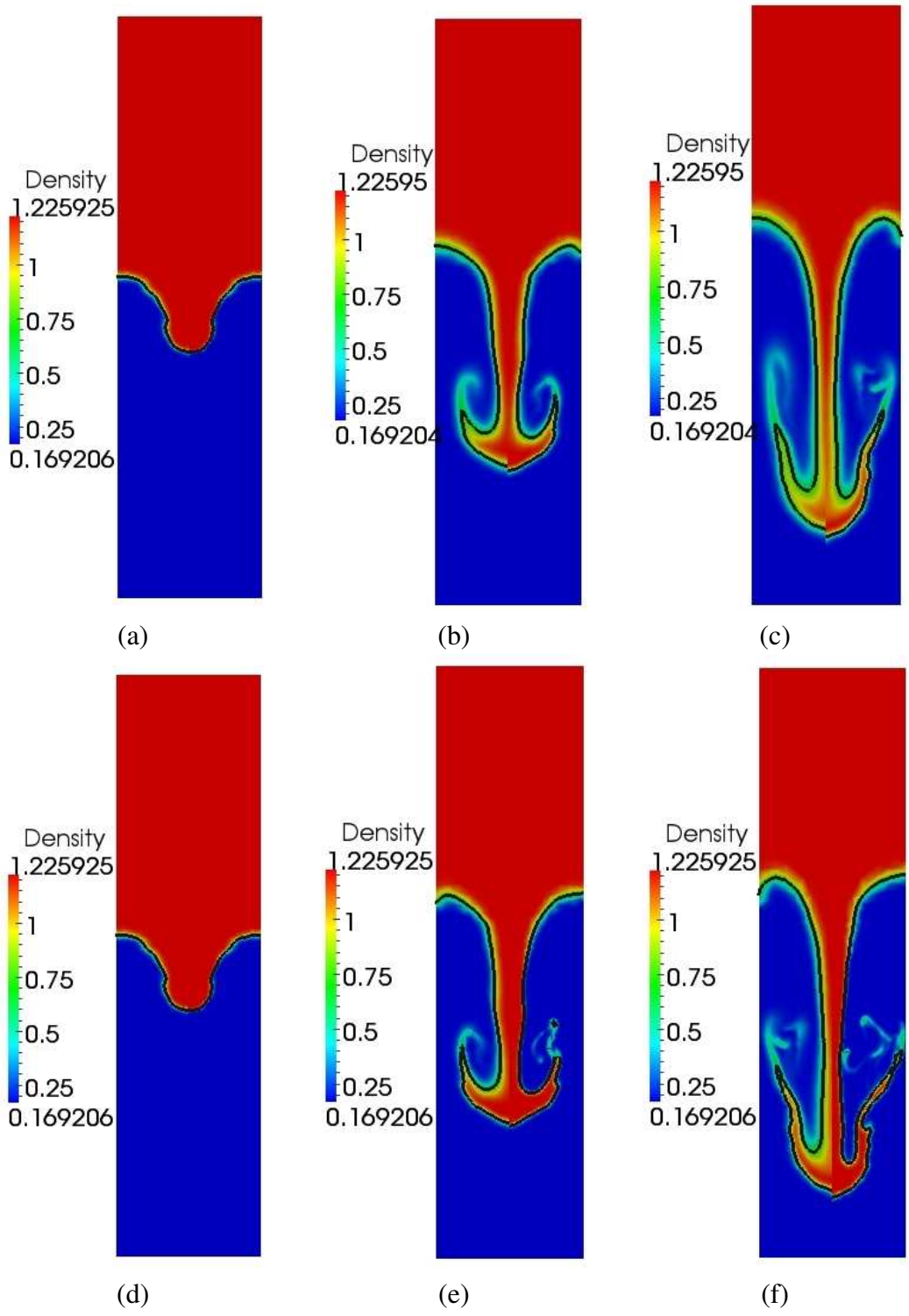

Figure 11: Rayleigh-Taylor instability. Pictures (a), (b), (c) are a comparison of the DG^0 (left) and DG^1 (right) approximations, taken at time $t = 0.2$, $t = 0.6$, $t = 0.8$. Pictures (d), (e), (f) are comparisons between DG^1 (left) and DG^2 (right) at the same times.

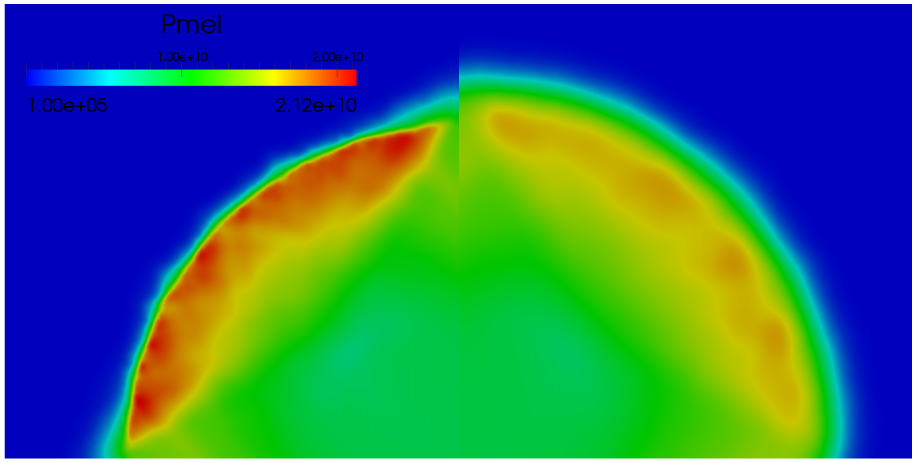

Figure 12: Detonation front: comparison of the DG^0 (right) and the DG^1 (left) solution. The permeable front is clearly better described with the latter scheme.

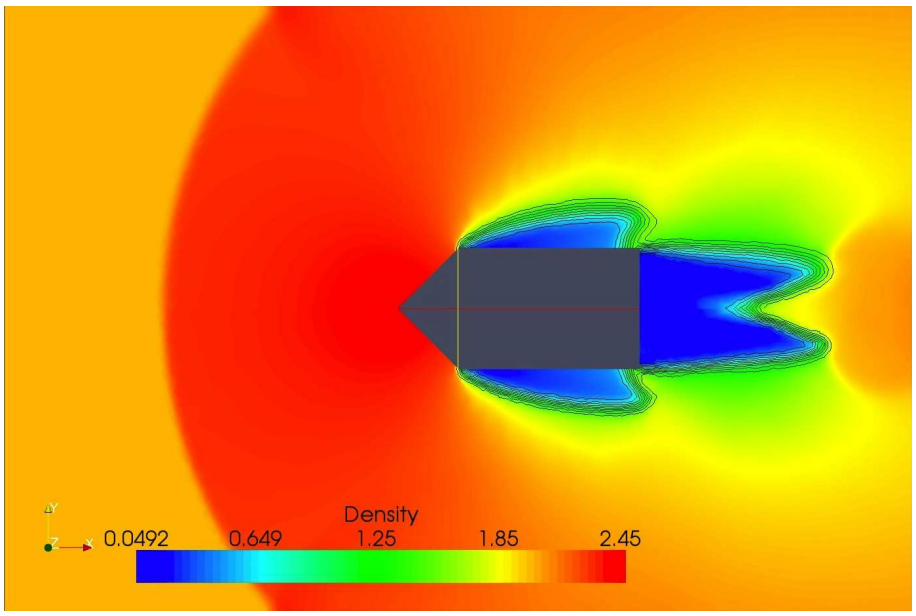

Figure 13: Phase transition front: comparison of the DG^0 (top) and the DG^1 (bottom) solution. Isovalues of the volume fraction are also presented in black lines. The permeable front is clearly better described with the latter scheme.

REFERENCES

[1] E. Franquet and V. Perrier. Runge–Kutta discontinuous Galerkin method for the approximation of Baer & Nunziato type multiphase model. *Journal of Computational Physics*, 231(11):4096–4141, 2012.

[2] E. Franquet and V. Perrier. Runge–Kutta discontinuous Galerkin method for interface flows with a maximum preserving limiter. *Comput. & Fluids*, 2012. Accepted.

[3] E. Franquet and V. Perrier. Runge–Kutta discontinuous Galerkin method for reactive multiphase flows. 2012. Submitted.

[4] R. Abgrall and R. Saurel. Discrete equations for physical and numerical compressible multiphase mixtures. *Journal of Computational Physics*, 186(361-396), 2003.

[5] M.R. Baer and J.W. Nunziato. A two-phase mixture theory for the deflagration-to-detonation transition (ddt) in reactive granular materials. *Int. J. Multiphase Flows*, 12(12):861–889, 1986.

[6] Nikolai Andrianov and Gerald Warnecke. The Riemann problem for the Baer-Nunziato two-phase flow model. *J. Comput. Phys.*, 195(2):434–464, 2004.

[7] Vincent Deledicque and Miltiadis V. Papalexandris. An exact Riemann solver for compressible two-phase flow models containing non-conservative products. *J. Comput. Phys.*, 222(1):217–245, 2007.

[8] Michael Dumbser, Arturo Hidalgo, Manuel Castro, Carlos Parés, and Eleuterio F. Toro. FORCE schemes on unstructured meshes II: Non-conservative hyperbolic systems. *Comput. Methods Appl. Mech. Engrg.*, 199(9-12):625–647, 2010.

[9] S. Rhebergen, O. Bokhove, and J. J. W. van der Vegt. Discontinuous Galerkin finite element methods for hyperbolic nonconservative partial differential equations. *J. Comput. Phys.*, 227(3):1887–1922, 2008.

[10] D.A. Drew and S.L. Passman. *Theory of multicomponent fluids*, volume 135 of *Applied Mathematical Sciences*. Springer-Verlag, New York, 1999.

[11] Robert J. Adler. *The geometry of random fields*. John Wiley & Sons Ltd., Chichester, 1981. Wiley Series in Probability and Mathematical Statistics.

[12] Athanasios Papoulis and Unnikrishna S. Pillai. *Probability, Random Variables and Stochastic Processes*. McGraw-Hill Science/Engineering/Math, December 2001.

[13] Gianni Dal Maso, Philippe G. Lefloch, and François Murat. Definition and weak stability of nonconservative products. *J. Math. Pures Appl. (9)*, 74(6):483–548, 1995.

[14] J.J. Quirk and S. Karni. On the dynamics of a shock-bubble interaction. *Journal of Fluid Mechanics*, 318:129–163, 1996.

[15] J.-F. Haas and B. Sturtevant. Interactions of weak shock waves with cylindrical and spherical gas inhomogeneities. *Journal of Fluid Mechanics*, 181:4l–76, 1987.

[16] R.R. Nourgaliev, T.N. Dinh, and T.G. Theofanous. Adaptive characteristics-based matching for compressible multifluid dynamics. *Journal of Computational Physics*, 213(2):500 – 529, 2006.

[17] Xiangxiong Zhang and Chi-Wang Shu. On maximum-principle-satisfying high order schemes for scalar conservation laws. *J. Comput. Phys.*, 229(9):3091–3120, 2010.

[18] Xiangxiong Zhang, Yinhua Xia, and Chi-Wang Shu. Maximum-principle-satisfying and positivity-preserving high order discontinuous Galerkin schemes for conservation laws on triangular meshes. *Journal of Scientific Computing.*, 50(1):29–62, 2012.

[19] Steven T. Zalesak. Fully multidimensional flux-corrected transport algorithms for fluids. *J. Comput. Phys.*, 31(3):335–362, 1979.

[20] Alfredo Bermudez and Ma. Elena Vazquez. Upwind methods for hyperbolic conservation laws with source terms. *Comput. & Fluids*, 23(8):1049–1071, 1994.

[21] O. Le Métayer, J. Massoni, and R. Saurel. Modelling evaporation fronts with reactive Riemann solvers. *Journal of Computational Physics*, 205:567–610, 2005.